Canadian Science Publishing
NRC Research Press journals | Publishing Services

Canadian Geotechnical Journal
Revue canadienne de géotechnique

Axial load testing of helical pile groups in a glaciolacustrine clay

Journal:	*Canadian Geotechnical Journal*
Manuscript ID	cgj-2017-0425.R1
Manuscript Type:	Article
Date Submitted by the Author:	17-Jan-2018
Complete List of Authors:	Lanyi-Bennett, Stephen; University of Alberta, Civil & Environmental Engineering Deng, Lijun; University of Alberta, Department of Civil and Environmental Engineering
Keyword:	helical piles, screw piles, pile groups, full-scale load testing, soil setup
Is the invited manuscript for consideration in a Special Issue? :	N/A

Axial Load Testing of Helical Pile Groups in a Glaciolacustrine Clay

Stephen A. Lanyi-Bennett[1] and Lijun Deng[2]

Corresponding Author:

Lijun Deng

Department of Civil & Environmental Engineering

University of Alberta

9203 - 116 St NW

Edmonton, Canada T6G 1R1

Phone: (780) 492 – 6210

Email: ldeng@ualberta.ca

---

[1] MSc student, Department of Civil and Environmental Engineering, University of Alberta, Edmonton, Canada, T6G 1R1, slanyi@ualberta.ca

[2] Assistant Professor, Department of Civil and Environmental Engineering, University of Alberta, Edmonton, Canada, T6G 1R1, ldeng@ualberta.ca, 1-780-492-6210

ABSTRACT

The behaviour of helical pile groups has not previously been experimentally investigated through field testing. In the present study, field compressive load tests of 2 × 2 helical pile groups and single piles were conducted in a glaciolacustrine clay in Edmonton, Canada. The group pile spacing, inter-helix spacing, and soil setup time were varied. Piezometers were used to measure the excess pore pressure (u_e) response to pile installation. Selected groups contained a strain gauge instrumented pile that was used to estimate the pile load transfer and failure mechanism. Group performance was evaluated by estimating the group efficiencies and settlement ratios. Results show that the group interaction of small diameter helical piles was lower than that of conventional pile groups. The short-term performance of groups was significantly reduced by u_e and groups with smaller group pile spacing had a greater reduction in short-term performance. Instrumented grouped piles and one single pile, both having an inter-helix spacing ratio of 5, exhibited individual bearing failure. The measured group capacities and load distributions indicated that individual pile failure occurred, as opposed to block failure.

Key words: helical piles, screw piles, pile groups, full-scale load testing, soil setup, cohesive soil

INTRODUCTION

A helical pile is a deep foundation element composed of one or more steel helical bearing plates welded to a central steel shaft. Piles are screwed into the ground by applying torque and axial force, delivered by a hydraulic drive head. This pile type has various advantages over conventional piles with consistent cross-sections. These advantages include: fast installation, light-weight and mobile installation equipment, low noise and vibration during installation, minimal soil disturbance, and pile reusability.

To resist larger loads, helical piles are commonly installed in groups. The application of helical pile groups is especially common for power transmission tower foundations (Adams and Klym 1972). Despite the wide application of helical pile groups, their engineering behaviour has not been established in literature. The present study aims to further the understanding of helical pile group behaviour by performing full-scale field load tests. The specific objectives of this research are to investigate the helical pile group: load-settlement response, installation-induced pore pressure response, effects of soil setup, and failure mode.

BACKGROUND

General Pile Group Behaviour

Past studies (Whitaker 1957; Meyerhof 1960; Poulos 1968; Chen et al. 2011; Dai et al. 2012) have shown that grouped piles interact such that their performance under loading is altered. This phenomenon is known as the group effect. Group performance is often evaluated based on the ultimate group capacity and the group load-settlement behaviour. The group effect causes a reduction in group performance due to the overlapping of stress and strain fields of neighbouring piles. The degree of group interaction increases with decreasing pile spacing, increasing pile length to diameter ratio, and the increasing number of piles in a group (Poulos 1989). Two

metrics are commonly used to evaluate pile group performance: the group efficiency (η_g) and the settlement ratio (R_s). Group efficiency quantifies the reduction in ultimate group capacity; it is defined as (Whitaker 1957):

$$\eta_g = \frac{Q_{ug} / N}{Q_{us}} \quad (1)$$

where Q_{ug} is the ultimate group capacity, Q_{us} is the ultimate single pile capacity, and N is the number of piles in the group; the numerator is termed the average group capacity. To evaluate group performance based on settlement, the settlement ratio (R_s) has been adopted for this study, defined as (Poulos and Davis 1980):

$$R_s = \frac{S_g}{S_s} \quad (2)$$

where S_g is the settlement of a pile group center and S_s is the settlement of a single pile, evaluated when the average group load equals the single pile load.

There are two possible failure mechanisms for grouped piles: block failure and individual pile failure. Block failure occurs when the soil between grouped piles fails as a block, while individual failure is characterized by local pile penetration (Whitaker 1957). The likelihood that block failure occurs is higher for groups with closer pile spacing and longer piles and for groups in cohesive soils (Salgado 2008).

Helical Pile Group Behaviour

The group behaviour of helical piles may differ from that of conventional piles due to the unique geometry of this pile type. For helical piles, the helix diameter is always larger than the shaft diameter, while straight shaft concrete piles and driven piles often have cylindrical shafts with an equal-diameter toe and shaft. Group pile spacing is often described by the ratio of the pile center-to-center spacing (s_g) to pile toe diameter (D) for conventional pile groups, or to the

helix diameter (D) for helical pile groups. At equal s_g/D ratios, the shaft spacing within helical pile groups will be greater than in conventional pile groups. Figure 1 shows a conceptual schematic of the stress fields around a conventional pile group and a helical pile group. Both groups have equal s_g/D ratios; however, the shaft diameter (D) of the conventional pile group is greater than that of the helical pile group (d), thus, resulting in less shaft interaction in the helical pile group.

Trofimenkov and Mariupolskii (1965) performed field pullout tests on groups consisting of three helical piles in a row and found that there was no group resistance reduction when $s_g/D \geq 1.5$. Shaheen and Demars (1995) performed laboratory pullout tests of model anchor groups in sand. They determined that in dense sand helical pile group capacity reduced exponentially as group pile spacing decreased; in loose sand, however, group performance was independent of group pile spacing. Elsherbiny (2011) evaluated helical pile group performance using the finite element method (FEM). It was found that η_g of a 2×2 helical pile group was greater than that of conventional pile groups because soil displacement around the helices was localized. Perko (2009) suggested that the soil in the inter-helix region between grouped piles may fail as a block, and that Q_{ug} may be estimated by summing the bearing resistance of the base of the block and the soil shear resistance along sides of the block:

$$Q_{ug} = q_{b,ult} m_1 m_2 + 2 s_u (n-1)(m_1 + m_2) s \quad (3)$$

where $q_{b,ult}$ is the ultimate state unit base resistance of the block, m_1 and m_2 are the width and breadth of the group bounded by the helices, n is the number of helices per pile, s is the inter-helix spacing, and s_u is the undrained shear strength of soil.

Installation Disturbance and Soil Setup in Cohesive Soils

The screwing action during helical pile installation causes soil to displace outward from the pile shaft and to be sheared by the helical plates cutting through the soil. This installation disturbance causes a change in the soil stress state near the pile and may alter the shear strength of fine-grained soils (Weech 2002). The change in soil stress may be the result of two factors: the increase in total stress, caused by the penetration of the pile shaft forcing soil radially outward from the shaft (Poulos and Davis 1980), and the change in effective stress due to the volumetric response of fine-grained soils to shear strain (Randolph 2003). The increase in total stress will result in positive excess pore pressure (u_e), but a soil's response to shear strain depends on the overconsolidation ratio (OCR) (Weech 2002). Since s_u is dependent on the magnitude of u_e, s_u will vary as pore pressure equilibrates. The dissipation of u_e, resulting in an increase in pile capacity with time, is known as soil setup. The rate of soil setup is directly related to the rate of consolidation near the pile (Soderberg 1962). Weech (2002) conducted a field investigation on the soil disturbance caused by a single helical pile installation in a highly-sensitive marine clay. Weech (2002) measured u_e at various distances away from the pile shaft and determined pile capacities at several setup times, where the setup time (t_s) is the time between pile installation and loading.

Pile grouping may alter the u_e regime in the vicinity of a pile group. Soderberg (1962) noted that as group pile spacing decreases, u_e near the piles increases due to the compounding influence of closely spaced piles. Thus far, soil setup and the interaction between u_e and group performance has not yet been investigated for helical pile groups.

Helical Pile Load Distribution - Individual Bearing Model

An axially-loaded helical pile's failure surface can be described by the individual bearing model (IBM) or the cylindrical shear model (CSM) (Zhang 1999). The IBM predicts that bearing failure occurs at each helix and that there is negligible interaction between adjacent helices (Elkasabgy and El Naggar 2015). Past studies have found that the IBM dominates pile behaviour when the ratio of the vertical helix spacing (s_h) to D is greater than 1.5 (Rao et al. 1993; Rao and Prasad 1993) or 3 (Zhang 1999; Tappenden 2007). The ultimate capacity (Q_{us}) predicted by the IBM in an undrained condition is estimated as:

$$Q_{us} = Q_{bearing} + Q_{shaft} = N_t s_u A_b n + \alpha s_u \left(\pi d H_{eff}\right) \quad (4)$$

where $Q_{bearing}$ is the sum of bearing resistance of all helical plates, Q_{shaft} is the shaft resistance, N_t is a bearing capacity coefficient, A_b is the helical plate bearing area, α is the adhesion coefficient, d is the shaft diameter, and H_{eff} is the effective shaft length. The CFEM (2006) suggests an N_t value of 9 when the pile toe diameter is less than 0.5 m and α between 0.5 and 1.0. Perko (2009) suggests a lower α for helical piles due to poor soil-shaft contact caused by the shaft wobbling during pile installation. H_{eff} is the length of shaft that contributes to Q_{shaft}; it can be estimated as the shaft length above the lower helix (H_s) minus 1D per helix, to account for a void forming above each helix (Elkasabgy and El Naggar 2015).

Torque – Capacity Relationship

Research has shown that the installation torque measured during pile installation can be used as an indicator of the shear strength of soil traversed by the pile and the pile's capacity. Hoyt and Clemence (1989) developed an empirical equation relating the final installation torque (T) to ultimate capacity (Q_{us}) of a single helical pile:

$$Q_{us} = K_t \cdot T \quad (5)$$

where K_t is the capacity-torque ratio.

TEST SITE AND INVESTIGATION

The testing program took place at a cohesive soil site at the University of Alberta farm in Edmonton, Canada. The subsoils in this area consist of Glacial Lake Edmonton sediments overlying till, representing a typical soil profile of the Edmonton area. The glaciolacustrine sediments were deposited near the end of the Wisconsin glacial period, as a result of the formation of Glacial Lake Edmonton, approximately 12,000 years ago (Godfrey 1993).

A comprehensive site investigation was conducted prior to and during the testing program, which included cone penetration testing (CPT), Shelby tube sampling, lab soil testing, and piezometer installations. Figure 2 shows the locations of the site investigation activities with respect to the test pile locations.

The soil stratigraphy profile was determined using CPT data and laboratory characterization testing of sampled soils. Previous knowledge of the site geology (Bayrock and Hughes 1962) and a review of past investigations near the site (Zhang 1999; Tappenden 2007) also assisted in interpreting the soil layers. As shown in Figure 3, beneath 0.7 m of topsoil, there is a 0.8-m-thick clayey silt crust underlain by a 4.5-m-thick stiff glaciolacustrine clay deposit. At a depth of 6.0 m there exists a 1.5-m-thick layer of interbedded silty clay with sand seems. From 7.5 to 9.5 m below the ground surface, the soil consists of a silty sand deposit with interbedded silty clay; this layer is underlain by till at a depth of 9.5 m. Throughout the testing program, the groundwater table (GWT) depth was measured directly with a piezometer. It was found that the GWT varied from 3.0 m deep in September to 4.0 m deep in December 2016.

Laboratory soil classification testing and strength testing was conducted on soil from boreholes BH-1 to BH-4, from depths between 0.75 and 6.55 m. Soil classification testing

included: Atterberg limits, moisture content (w), bulk unit weight (γ_b), and specific gravity of solids (G_s). To determine s_u, unconfined compressive strength (UCS) testing was performed. Consolidation testing was performed on two samples from BH-5, at depths of 4.72 and 5.33 m. Figure 3a shows a summary of the lab test results.

Equation 6 (Robertson and Cabal 2015) was used to estimate the in-situ s_u of the cohesive soil at this site:

$$s_u = \frac{q_t - \sigma_v}{N_{kt}} \tag{6}$$

where q_t is the corrected cone tip resistance, σ_v is the overburden stress, and N_{kt} is an empirical factor (typically ranging from 10 to 18, Robertson and Cabal 2015) that typically increases with a soil's plasticity. Based on findings from a previous investigation near this site (Tappenden 2007), an N_{kt} value of 18 was used; also, using an N_{kt} value of 18 resulted in good agreement between the in-situ s_u and laboratory-measured s_u (Figure 3d). UCS tests of the saturated stiff clay (CH) layer found s_u to vary between 55 and 67 kPa, whereas s_u estimated from Equation 6 varied between 57 and 77 kPa.

LOAD TEST PROGRAM

The field test program consisted of axial compression loading of seven 2 × 2 helical pile groups and four single piles. Testing was conducted from September to December of 2016.

Test Pile and Load Test Description

Double-helix test piles were manufactured and installed for this project. All test piles had a length (L) of 6.10 m, a closed-ended shaft of 73-mm-diameter (d), two 305-mm-diamter helices (D), a helix pitch of 102 mm, and an inter-helix spacing (s_h) of 914 mm or 1524 mm. Figure 4 shows a schematic of the test pile geometries and the location of the helices with respect to the soil stratigraphy.

Table 1 shows a summary of all pile tests. Groups with an s_h/D ratio of 3 (PG-A1 to PG-C2 in Table 1) had varied group-pile-spacing ratios (s_g/D = 2, 3, and 5). For groups with an s_g/D ratio of 2 and 3, the soil setup time (t_s) was also varied. Tests PG-B2 and PG-C2 occurred 5 hr after pile installation, while tests PG-B1 and PG-C1 occurred 8 to 9 days after pile installation. The single pile tests P-2 and P-3 (s_h/D = 3) were performed to compare the load-settlement response of single piles to that of pile groups.

Instrumentation

Drive-point vibrating wire piezometers were used to measure the pile installation-induced u_e generation and dissipation at the center of groups PG-B1 and PG-C1 and near the single pile P-1. The baseline piezometer readings were also used to measure the depth of the GWT throughout the testing program. The piezometer consisted of a 25-mm-diameter hollow steel shaft with a coned tip. Figure 5 shows a schematic of the piezometer assembly and installation. The piezometer was screwed onto a drill rod to allow the assembly to reach the desired depth. Before installing the piezometers, a 150-mm-diameter borehole was drilled with an auger to a depth of 3.7 m, and cased with a steel pipe to prevent soil sloughing. The piezometer was then placed into the steel pipe and pushed the remaining 1.0 to 1.5 m to the target depth. The borehole was required because pushing the piezometer from the surface may have over-ranged the vibrating wire diaphragm. All piezometers were installed at least one week prior to pile installation to allow the pore pressure generation caused by the instrument installation to fully dissipate. For the group tests, the depth of the piezometer tip was 5.2 m below the ground surface, or 500 mm below the upper-helix; for the single pile P-1, the depth of the piezometer tip was 4.5 m below ground surface, or 250 mm above the upper-helix.

One of the four piles in PG-D1 and PG-D2, and the single pile P-4, were instrumented with electrical resistance strain gauges at four stations along the pile shafts. Figure 4 shows a schematic of the strain gauge stations (SG-1 to SG-4) on a test pile. With this gauge configuration, the load resisted by each pile component (upper-shaft, upper-helix, inter-helix, lower-helix) could be resolved. A Wheatstone full-bridge circuit was used at each station. To prevent damage to the gauges during pile installation, steel covers were used at the gauge locations. The covers consisted of two hollow half-cylinder steel pieces that fit together around the shaft to form a continuous steel barrier. The covers were 100 mm long and 15 mm thick. To fasten the covers to the shaft, a threaded rod ran through the cover and the shaft through clear drill holes and was bolted at both ends. Because of the bolting method, the covers did not change the shaft stiffness at the gauge stations. Before installing the covers, an epoxy and a polymer-based water-resistant coating were applied to the gauges surface.

A 980-kN-capacity hydraulic jack was used to apply a load to the test piles. A load cell was used to measure the applied load. Axial pile displacements were measured using linear potentiometers (LPs). For pile group tests, one LP was installed at each of the group's four corners, shown in Figure 6; for single piles, one LP was fastened to either side of the loading plate. The LPs and the load cell were calibrated prior to the testing program. A data logger, with a 5-sec sampling interval, was used to record the measurements. Installation torque was measured with an electronic torque monitor and recorded manually every 0.3 m of pile penetration.

Load Test Configuration

A typical configuration is shown in Figure 5. The reaction beam was a 7-m-long W840×299 I-beam and the reaction piles were spaced 5.8 m apart (Figure 2). The reaction piles for pile group

tests were 7.9 m long, with a shaft diameter of 140 mm and four helices of 457-mm diameter; the reaction piles for individual pile tests were 6.1 m long, with a shaft diameter of 140 mm and three helices of 457-mm diameter. The reaction piles were over-designed to have a minimum capacity of 2.5 times the maximum design load. During pile testing, no axial displacements of the reaction piles were observed. Pile groups were centered between adjacent reaction piles; single test piles were spaced 1.52 m apart, with at most two test piles centered between two reaction piles (Figure 2). The minimum center-to-center spacing between test and reaction piles was five helix diameters of the larger pile.

A pile cap was required for pile group tests. The cap consisted of three I-beams configured in an 'H' pattern, as shown in Figure 6. The two lower-cap I-beams (W250×49), running parallel to the reaction beam, had slotted bottom flanges so they could be fastened, using four bolts, to the loading plates of the test piles below. The upper-cap I-beam (W310×97) was seated at the center of the two lower beams, aligned perpendicular to the reaction beam.

Due to the pitch of the helices, a single helical pile may rotate under axial loading. In practice, this rotation is unlikely because the pile cap is usually fixed to the superstructure. To prevent pile rotation during single pile tests, a collared loading plate with a hooked end was bolted to each test pile. A chain was connected to the hook on the loading plate and wrapped around the nearest reaction pile. The chain was then tightened to provide a moment to resist pile rotation.

Load Test Procedure

All pile testing followed the ASTM (2013) "quick test" axial compression load test procedure (D1143/D1143M – 07). The applied load was increased in increments of approximately 5% of the estimated design load. During each increment, the load was held for 5 min to allow the rate of pile settlement under the sustained load to approach zero. When the applied load was less than

or equal to the ultimate load, the measured creep settlement was negligible after the 5 min wait period. Individual piles were loaded until additional settlement resulted in no further increase in pile resistance (known as plunging failure). For pile group tests it was not always possible to reach plunging failure. Differential settlement between piles in the groups caused tilting of the hydraulic jack as the piles approached plunging. For groups with excessive differential settlement, testing progressed until it was deemed no longer safe to increase the load. After reaching the maximum load, unloading occurred in five approximately equal decrements.

RESULTS AND DISCUSSION

Selection of Failure Criterion

For single pile testing, failure is generally defined by the limit load, i.e. the load causing plunging. However, for this study, differential settlement between grouped piles prevented the groups from reaching the limit load during testing. The differential pile settlement was likely caused by eccentric loading of the groups and varied soil stiffness between grouped piles. Eccentric loading was likely the main cause of the differential settlement, as the CPT Soil strength interpretation and UCS testing from across the site (Figure 3d) indicate low soil strength variability. The magnitude of the differential settlement was likely accentuated by the relatively small diameter, low capacity test piles. Efforts were made to mitigate eccentric loading by installing all grouped piles to the same elevation and by applying the load as close as possible to the group's center; however, differential settlement still occurred to an extent. As differential pile settlement prevented groups from reaching the limit load, a settlement-based failure criterion was adopted for this study. Elkasabgy and El Naggar (2015) recommended that the ultimate load (Q_u) should fall within the nonlinear region of the load-settlement curve, where creep settlement is low. Based on this recommendation and from inspection of the load-settlement curves, Q_u

adopted for this study was defined as the load causing pile settlement of 5% of the helix diameter, or 15.2 mm. This 5%*D* criterion was also adopted for the helical pile study by Elsherbiny and El Naggar (2013). At 5%D, creep settlement was negligible and differential settlement between grouped piles was smaller than at loads near the onset plunging. The individual pile settlement of each pile group, measured at the ultimate group load, is shown in Table 2.

Figure 7 shows the load-settlement curves for the pile groups and single piles P-2 and P-3. For pile groups, the applied group load was plotted against the settlement of the pile group center, determined using the LP readings at the group's corners. Following the 5%*D* criterion, Q_u of all applicable tests are summarized in Table 1.

Group test repeatability was found to depend largely on limiting eccentric loading, thereby, reducing differential pile settlements. The loading of PG-A1 was stopped shortly after reaching Q_u due to the onset of eccentric loading, which was likely accentuated by the large group pile spacing ($s_g/D = 5$) of this group. The performance of PG-D1 and PG-D2 ($s_h/D = 5$) could not be evaluated due to excessive differential settlement between the grouped piles. PG-D1 and PG-D2 were the first group tests performed and less care was taken in ensuring that all piles in the groups were installed to the same elevation prior to loading. From the initiation of loading, these groups settled unevenly, resulting in large differential settlements (Table 2) and tilting of the hydraulic jack. The load vs. displacement curves resulting from these tests did not accurately represent the pile group behaviour; therefore, the performance of these groups was not analyzed.

Metrics of Group Performance

To quantify the group effect and to evaluate pile group performance, the load-settlement curves of the groups were compared to that of P-2 and P-3. A capacity-based evaluation was made by calculating η_g (Equation 1). A settlement-based evaluation was made by calculating R_s (Equation

2) at selected pile group factors of safety (FS), where FS was defined as the ratio of the measured Q_{ug} to the pile group load (Q_g). The pile group and single pile load-settlement behaviour could not be directly compared without considering T, since T is proportional to pile capacity. To mitigate the effect of T on η_g and R_s, the pile group load (Q_g) and single pile load (Q_s) were normalized. The value of Q_g was normalized by the sum of the estimated ultimate capacities of the single piles in each group, which were calculated using the torque-capacity relationship (Equation 5), as shown in Equation 7:

$$\overline{Q}_g = \frac{Q_g}{\sum_{i=1}^{N}\left(K_t \cdot T_i\right)} \tag{7}$$

The K_t factor used in Equation 7 was an average (23.65 m^{-1}) determined from P-2 and P-3 (Table 1). The normalized single pile load ($\overline{Q}_s$) was calculated using Equation 8:

$$\overline{Q}_s = \frac{Q_s}{Q_{us}} \tag{8}$$

where Q_{us} is the measured ultimate capacity of single piles.

The normalized loads $\overline{Q}_s$ and $\overline{Q}_g$ were plotted against settlement (Figure 8). After normalization, the P-2 and P-3 curves became very consistent. The value of η_g equals the ratio of $\overline{Q}_g$ to the average $\overline{Q}_s$ of P-2 and P-3 at a settlement of 5%D (15.2 mm). The value of R_s equals the ratio of S_g to the average S_s of P-2 and P-3 at equal normalized loads ($\overline{Q}_g = \overline{Q}_s$), at a given pile group FS.

Effects of the s_g/D ratio on Group Performance

The effects of group pile spacing on group performance were investigated by performing group load tests with varied s_g/D ratios. Pile group tests PG-A1, PG-B1, and PG-C1 with s_g/D

ratios of 5, 3, and 2, respectively, were carried out; these groups had s_h/D ratios of 3. All these tests had a $t_s \geq 7$ days to allow for complete u_e dissipation (discussed later). To compare the performance of helical groups to conventional pile groups, η_g was estimated using the Converse-Labarre equation (Equation 9, Bolin 1941), an empirical formula commonly used to estimate η_g of conventional piles (Hanna et al. 2004):

$$\eta_g = 1 - \frac{\theta\left[(N_1 - 1)N_2 + (N_2 - 1)N_1\right]}{90 N_1 N_2} \quad (9)$$

where $\theta = \arctan(D/s_g)$, N_1 is the number of rows in a group, and N_2 is the number of columns.

Figure 9 shows η_g of the three tests along with η_g estimated using the Converse-Labarre equation and η_g estimated by Elsherbiny (2011). The results from this study were compared to the results from Elsherbiny (2011) because the soil properties, pile geometries, and group configurations from both studies were similar (Elsherbiny: s_u = 75 kPa, L = 6.2 m, d = 273 mm, D = 610 mm, n = 2, s_h/D = 3, 2×2 group); although, Elsherbiny's study was performed using finite element analysis. Figure 9 shows that η_g decreased with a deceasing s_g/D ratio; the values of η_g were 96.8%, 95.5%, and 90.7% at s_g/D ratios of 5, 3, and 2, respectively. The magnitude and trend of the measured η_g matched closely with Elsherbiny (2011) predicted values, although the measured values were 1 to 2 percentage points higher. The measured η_g values were consistently much higher than the Converse-Labarre equation predicted values, indicating that the interaction of helical piles groups was lower than that of conventional pile groups with equal s_g/D ratios.

Figure 10 shows the measured R_s for PG-A1, PG-B1, and PG-C1 plotted at pile group FS of 1, 1.5, and 2. The values of R_s were only estimated up to the group FS of 2 because the values of S_g and S_s at loads corresponding to FS > 2 were so small (< 1 mm) that the accuracy of R_s was low.

At all FS values, R_s was found to increase with a decreasing s_g/D ratio. At FS of 1 (i.e. at Q_{ug}), R_s was 1.88, 1.38, and 1.26 at s_g/D ratios of 2, 3, and 5, respectively. At higher FS (lower load), R_s was reduced, indicating lower group interaction. At FS of 2, all groups had a value of R_s below 1.0, indicating that the groups had a stiffer response than the single piles under low loads.

Installation-Induced Pore Pressure

Pile installation-induced u_e was measured for P-1, PG-B1, and PG-C1. For P-1, the piezometer was installed at a radial distance (r) of 450 mm from the shaft center, corresponding to a r/r_{shaft} ratio of 12.3, where r_{shaft} is the pile shaft radius. For PG-B1 and PG-C1, piezometers were installed at the center of the groups, where r of PG-B1 and PG-C1 were 645 mm (r/r_{shaft} = 17.7) and 430 mm (r/r_{shaft} = 11.8), respectively. The u_e time histories of PG-B1 and PB-C1 were used to interpret the behaviour of PG-B2 and PG-C2. It was deemed appropriate to do so because the pile geometry and embedment depth were consistent for all piles and the site was considered relatively homogenous.

Figure 11 shows the measured u_e normalized by the initial vertical effective stress (σ'_{v0}) versus the time after the initiation of the pile group installation; the inset figure shows the curves of the first 24 hr and labels the instant when load testing began. The duration of a pile group installation varied between 0.75 and 1 hr. The inset in Figure 11 shows that the instantaneous u_e response to pile installation was negligible; also, the u_e response to the applied load during testing was negligible. Cavity expansion theory explains that after pile installation there is a region around the pile shaft that is plastically deformed. Within the plastic zone, the instantaneous u_e decreases logarithmically with distance from the pile shaft and reaches zero outside the plastic zone (Randolph and Wroth 1979; Gibson and Anderson 1961). Following Randolph and Wroth (1979), the radius of the plastic zone in the present study was estimated as

$10r_{shaft}$ to $14r_{shaft}$, given an estimated G/s_u of 100 to 200 (Duncan and Buchignani 1987), where G is the soil shear modulus. In the present study, the instantaneous u_e was negligible because the piezometers were on the verge of, or outside, the plastic zone ($r/r_{shaft} \geq 11.8$). Further, the low sensitivity of the stiff clay also depressed the generation of u_e (as observed by Poulos and Davis 1980).

After pile installation, u_e started to increase, which was also predicted by Randolph and Wroth (1979) for soils on the verge of or outside the plastic zone. There was a significant delay (16 to 25 hr) between the initiation of pile installation and measuring a peak u_e. The time lag to the peak u_e was caused by a hydraulic gradient between the piles and the piezometer resulting in a redistribution of u_e away from the piles (Sully and Campanella 1994). The length of time lag to the peak measured u_e was longer for PG-B1 (25 hr) than for PG-C1 (16 hr) because the distance between the piles and piezometer (r/r_{shaft}) was greater for PG-B1 than for PG-C1. The maximum u_e response of the three tests was measured at PG-C1, where the u_e/σ'_0 ratio reached a peak of 0.288 (u_e = 24.0 kPa), for PG-B1, the peak measured u_e/σ'_0 ratio was 0.105 (u_e = 8.7 kPa), and for P-1, the peak u_e/σ'_0 ratio was 0.026 (u_e = 1.9 kPa). The measured u_e response for PG-B1 and PG-C1 was much greater than that of P-1, despite r/r_{shaft} of PG-B1 and PG-C1 being greater than or equal to r/r_{shaft} of P-1. The greater u_e response of PG-B1 and PG-C1 was due to the superposition of the zones of u_e generation at the group's centers. The higher u_e measured at PG-C1 than at PG-B1 was in part due to the closer proximity of the piezometer to the piles for PG-C1 than for PG-B1; also, the smaller s_g of PG-C1 may have caused more overlap in the zones of u_e generation between the grouped piles.

Figure 11 shows that the remaining u_e at t_s of PG-B1 (8 days) was negligible ($u_e/\sigma'_0 = 0.014$), and that u_e dissipation was complete at t_s of PG-C1 (9 days). This implies that the soil shear strength had fully recovered when these groups were tested.

Effects of Soil Setup on Group Performance

The effects of soil setup on group performance were evaluated by testing PG-B2 and PG-C2 at 5 hr after pile installation and comparing their performance to PG-B1 and PG-C1, which were tested 8 to 9 days after pile installation. Figure 9 shows the group efficiencies of these tests. The value of η_g for PG-B2 ($s_g/D = 3$) was 89.5%, which was a drop of 6.0 percentage points compared to η_g of PG-B1; η_g of PG-C2 ($s_g/D = 2$) was 78.5%, which was a drop of 12.2 percentage points compared to η_g of PG-C1.

Figure 10 shows the R_s versus FS of the tests described above. The values of R_s were consistently higher for the tests performed 5 hr after installation (PG-B2 and PG-C2) compared to the comparable tests performed at least 8 days after installation (PG-B1 and PG-C1). At FS of 1.0, R_s for PG-C2 and PG-C1 were 3.50 and 1.88, respectively, while for PG-B2 and PG-B1, R_s was 2.01 and 1.38, respectively. For all tests, R_s decreased with increasing FS (i.e. decreasing load).

The findings indicate that both group capacity and group settlement were significantly affected by u_e. As s_g decreased, the pore pressure distributions between neighbouring piles overlapped, resulting in a larger cumulative u_e response and larger temporary decrease in shear strength near the piles; thus, resulting in a temporary reduction in η_g and increase in R_s. These findings are corroborated by the measured u_e at the center of PG-B1 and PG-C1 (Figure 11).

Failure Mechanism and Load Transfer

The strain gauge data from PG-D1, PG-D2, and P-4 were used to estimate the load distributions along these piles. All piles involved had an s_h/D ratio of 5 and all group tests had an s_g/D ratio of 2. For all tests, t_s was at least 7 days to allow for complete u_e dissipation. The estimated load distributions were compared to the IBM-predicted (Equation 4) distribution to verify the pile failure mechanism. The parameters used in the calculation of the IBM-predicted distribution were: α of 0.3, N_t of 9, and s_u of 65 kPa in the stiff clay and topsoil and 100 kPa in the silty clay crust (Figure 3). Figure 12 shows the IBM–predicted distribution along with the measured distributions of the instrumented piles, shown at the ultimate state. The IBM closely predicted the load distribution of the grouped and single piles, as shown by the significant upper-helix bearing resistance and the relatively small inter-helix resistance of these piles.

To further investigate the pile load transfer, the ratio of the net bearing pressure (q_b) to s_u of both the upper and lower-helices were plotted against pile settlement. Net bearing pressure was calculated by dividing the measured helix resistance by the helix bearing area (A_b), where A_b of the lower-helix included the area of the shaft tip. Figure 13 shows the measured q_b/s_u trend of the helices of the instrumented piles. At the ultimate state, the measured q_b/s_u ratio is equal to the bearing capacity coefficient N_t, defined in Equation 10:

$$N_t = \frac{Q_{b,ult}}{A_b \cdot s_u} \tag{10}$$

where $Q_{b,ult}$ is the helix bearing resistance measured at the ultimate state.

Figure 13 shows that N_t of the lower-helices were greater than that of the upper-helices; N_t of the lower helices ranged between 7.7 and 10.4, while N_t of the upper helices ranged between 5.4 and 7.0. The reduction in N_t of the upper-helices is likely due to soil disturbance in the inter-helix

region during pile installation. As the helices cut through the inter-helix soil during installation the soil is partially destructured, whereas the soil below the lower-helices remains undisturbed (Elkasabgy and El Naggar 2015). The large variability of the measured N_t (between 5.4 and 10.4) suggests that the recommended value of 9.0 (Perko 2009; CFEM 2006) may not be representative of the bearing resistance of helical plates.

Evaluating the Group Failure Mechanism

The validity of the helical pile group block failure model (Perko 2009) was evaluated by comparing the measured Q_{ug} to the predicted Q_{ug} using Equation 3. For the predicted Q_{ug}, $q_{b,ult}$ was calculated as $9s_u$ (s_u = 65 kPa) following Perko's (2009) recommendation. Table 3 compares the measured and predicted Q_{ug} at various s_g/D ratios, for pile groups with complete u_e dissipation. The block failure model overestimated the group capacity in all cases, and the overestimation increased as the s_g/D ratio increased. This result indicates that block failure did not occur for any of these groups.

The load transfer data from PG-D1 and PG-D2 also indicate individual pile failure occurred, as significant upper-helix bearing resistance was measured for both tests (Figure 12). If block failure had occurred, the differential load between SG-2 and SG-3 should have been much smaller. As PG-D1 and PG-D2 had the lowest s_g/D ratio tested, it is likely that all other pile groups tested also exhibited individual pile failure, since block failure is less likely at larger s_g/D ratios.

CONCLUSIONS

Field load tests were conducted on seven helical pile groups and four single piles in a glaciolacustrine clay. The group pile spacing, inter-helix spacing, and soil setup time were varied among the tests. The following conclusions may be drawn:

1. The group efficiency (η_g) decreased as the s_g/D ratio decreased. The measured η_g of groups with a s_g/D ratio of 2, 3, and 5 were 90.7%, 95.5%, and 96.8%, respectively. The group interaction of small diameter helical piles is lower than that of conventional piles at equal s_g/D. The settlement ratio (R_s) increased as the s_g/D ratio decreased. At the group FS of 1.0, R_s was 1.88, 1.38, and 1.26 for groups with a s_g/D ratio of 2, 3, and 5, respectively; group interaction increased with increasing group load.
2. The instantaneous installation-induced u_e was negligible at the center of pile groups with s_g/D ratios of 2 and 3 (r/r_{shaft} = 11.8 and 17.7, respectively) and near the single pile (r/r_{shaft} = 12.3). After installation, u_e increased as pore pressure redistributed away from the piles.
3. The measured u_e at the center of groups exceeded the u_e measured near a single pile. For groups, the measured u_e at the groups center increased as the s_g/D ratio decreased.
4. Group performance was significantly affected by installation-induced u_e. Groups with s_g/D ratios of 2 and 3, which were tested at t_s of 5 hr, had significantly decreased η_g and increased R_s, when compared to groups tested at t_s of 8 to 9 days. This reduction in group performance increased as the s_g/D ratio decreased.
5. Single piles and pile groups (s_g/D = 2) containing piles with an s_h/D ratio of 5 exhibited individual bearing failure. The single and grouped instrumented piles indicated that more load was resisted by the lower-helix than the upper-helix. The measured N_t of the lower helices ranged between 7.7 and 10.4, while N_t of the upper helices ranged between 5.4 and 7.0.
6. The block failure model heavily overestimated the capacities of all test groups. Load distributions of the instrumented piles in PG-D1 and PG-D2 clearly showed that individual pile failure occurred.

ACKNOWLEDGMENT

This research was made possible in part from the support of the Natural Sciences and Engineering Research Council of Canada (NSERC), under the Engage Grants program (494853-16), and Roterra Piling Ltd. The authors would like to thank ConeTec Investigations Ltd. for performing CPT at the test site. We are thankful to Moira Guo, Zibo Shen, Chunhui Liu, students at the University of Alberta, for their assistance in laboratory soil testing. The first author would like to acknowledge the financial support of NSERC–Industrial Postgraduate Scholarship with the financial contribution of Roterra Piling Ltd.

REFERENCES

Adams, J. I., and Klym, T. W. 1972. A study of anchorages for transmission tower foundations. Can. Geotech. J., **9**: 89-104.

ASTM D1143M-07. 2013. Standard test methods for deep foundations under axial compressive load. ASTM International, West Conshohocken, PA.

Bayrock, L. A., and Hughes, G. M. 1962. Surficial Geology of the Edmonton District, Alberta. Rep. No. Preliminary Report 62-6, Research Council of Alberta, Edmonton, Alberta.

Bolin, H. W. 1941. The pile efficiency formula of the Uniform Building Code. Building Standards Monthly, **10**(1): 4-5.

Bowles, J. E. 1997. Foundation Analysis and Design, 5th ed. McGraw-Hill, Singapore.

Chen, S. L., Song, C. Y., and Chen, L. Z. 2011. Two-pile interaction factor revisited. Can. Geotech. J., **48**(5): 754-766.

CFEM. 2006. Canadian Foundation Engineering Manual. 4th ed. Canadian Geotechnical Society, BiTech Publisher Ltd., Canada.

Dai, G., Salgado, R., Gong, W., and Zhang, Y. 2012. Load tests on full-scale bored pile groups. Can. Geotech. J., **49**(11): 1293-1308.

Duncan, J. M., and Buchignani, A. L. 1987. Engineering Manual for Settlement Studies. Virginia Tech, Blacksburg, VA.

Elkasabgy, M., and El Naggar, M. H. 2015. Axial compressive response of large-capacity helical and driven steel piles in cohesive soil. Can. Geotech. J., **52**: 224-243.

Elsherbiny, Z. 2011. Axial and lateral performance of helical pile groups. Master's Thesis. University of Western Ontario, London, Canada.

Elsherbiny, Z., and El Naggar, M. H. 2013. Axial compressive capacity of helical piles from field tests and numerical study. Can. Geotech. J., **50**: 1191-1203.

Gibson, R. E., and Anderson, W. F. 1961. In situ measurement of soil properties with the pressuremeter. Civil Engineering and Public Works Review, **56**(658): 615-618.

Godfrey, J. D. 1993. Edmonton Beneath our Feet: a Guide to the Geology of the Edmonton Region. Edmonton Geological Society, Edmonton, Alberta.

Hanna, A. M., Morcous, G., and Helmy, M. 2004. Efficiency of pile groups installed in cohesionless soil using artificial neural networks. Can. Geotech. J., **41**: 1241-1249.

Hannigan, P. J., Rausche, F., Likins, G. E., Robinson, B. R., and Becker, M. L. 2016. Geotechnical Engineering Circular No. 12 – Volume I, Design and Construction of Driven Pile Foundations. Rep. No. FHWA-NHI-16-009, USDOT, D.C.

Hoyt, R. M., and Clemence, S. P. 1989. Uplift capacity of helical anchors in soil. 12th International Conference on Soil Mechanics and Foundation Engineering, Rio de Janeiro, Brazil, pp. 1019-1022.

Lanyi, S. A., and Deng, L. 2017. Effects of inter-helix spacing and soil setup on the behaviour of axially loaded helical piles in cohesive soil. Soils and Foundations, (in review).

Meyerhof, G. G. 1960. The design of franki piles with special reference to groups in sands. Symposium on Pile Foundations, 6th Congress Int. Assoc. Bridge and Struct. Eng. Stockholm.

Perko, H. A. 2009. Helical Piles: a Practical Guide to Design and Installation. J. Wiley, Hoboken, N.J.

Poulos, H. G. 1968. Analysis of the settlement of pile groups. Geotechnique, **18**: 449-471.

Poulos, H. G. 1989. Pile behaviour - theory and application. Geotechnique, **39**(3): 365-415.

Poulos, H. G., and Davis, E. H. 1980. Pile Foundation Analysis and Design. Wiley, New York.

Randolph, M. F. 2003. Science and empiricism in pile foundation design. Geotechnique, **53**(10): 847-875.

Randolph, M. F., and Wroth, C. P. 1979. An analytical solution for the consolidation around a driven pile. Int. J. Numer. Anal. Methods Geomech., **3**: 217-229.

Rao, N. S., and Prasad, Y. V. S. N. 1993. Estimation of uplift capacity of helical anchors in clays. J. Geotech. Eng., **119**(2): 352-357.

Rao, N. S., Prasad, Y.V.S.N., and Veeresh, C. 1993. Behaviour of embedded model screw anchors in soft clays. Geotechnique, **43**(4): 605-614.

Robertson, P.K., and Cabal, K.L. 2015. Guide to Cone Penetration Testing for Geotechnical Engineering. Gregg Drilling & Testing, Inc., Signal Hill, CA.

Salgado, R. (2008). The Engineering of Foundations. McGraw-Hill, New York.

Shaheen, W.A., and Demars, K.R. 1995. Interaction of multiple helical earth anchors embedded in granular soil. Marine Georesources and Geotechnology, **13**(4): 357-374.

Soderberg, L.O. 1962. Consolidation theory applied to foundation pile time effects. Geotechnique, **12**(3): 217-225.

Sully, J.P., and Campanella, R.G. 1994. Evaluation of field CPTU dissipation data in overconsolidated fine-grained soils. 13th International Conference on Soil Mechanics and Foundation Engineering, New Delhi, pp. 201-204.

Tappenden, K.M. 2007. Predicting the Axial Capacity of Screw Piles Installed in Western Canadian Soils. M.Sc. Thesis, University of Alberta, Edmonton, AB.

Trofirnenkov, J.G., and Mariupolskii, L.G. 1965. Screw piles used for mast and tower foundations. Proceedings of Sixth lnternational Conference on Soil Mechanics and Foundation Engineering, Montreal, QC, pp. 328-332.

Weech, C. 2002. Installation and Load Testing of Helical Piles in a Sensitive Fine-Grained Soil. M.Sc. Thesis. University of British Columbia, Vancouver, BC.

Whitaker, T. 1957. Experiments with model piles in groups. Geotechnique, **7**(4): 147-167.

Zhang, D. 1999. Predicting Capacity of Helical Screw Piles in Alberta Soils. M.Sc. Thesis. University of Alberta, Edmonton, AB.

FIGURE CAPTIONS

Figure 1. Conceptual schematic of stress fields around pile groups: (a) conventional pile group (adapted from Bowles 1997 and Hannigan et al. 2016); and (b) helical pile group.

Figure 2. Test site layout and site investigation activities. Test site location: Edmonton, Canada (53°29'54" N, 113°31'57" W).

Figure 3. (a) Site stratigraphy and lab test results summary; (b) CPT cone resistance profile; (c) CPT sleeve friction profile; and (d) undrained shear strength profile.

Figure 4. Test pile schematic with dimensions and strain gauge locations. Note: L, d, and D are equal for all test piles. Helix pitch is not drawn to scale.

Figure 5. Pile group load test setup and piezometer assembly schematic. Note: piezometer installation for group tests PG-B1 and PG-C1 only. Same setup was used for single pile tests except that the group cap assembly was not required.

Figure 6. Photo of a typical pile group test.

Figure 7. (a) Pile group load – settlement curves; (b) single pile load – settlement curves.

Figure 8. Pile group and single pile normalized load – settlement curves.

Figure 9. Group efficiency vs. group pile spacing ratio. Key parameters in Elsherbiny (2011): Q_u at $S = 5\%D$, $s_u = 75$ kPa, $L = 6.2$ m, $d = 273$ mm, $D = 610$ mm, $n = 2$, $s_h/D = 3$, and 2×2 group.

Figure 10. Settlement ratio vs. group pile spacing ratio at selected FS of pile groups.

Figure 11. Installation-induced pore pressure generation and dissipation for tests PG-B1, PG-C1, and P-1. Note: Test durations of PG-B2 and PG-C2 were approximately 2 hours.

Figure 12. Measured pile load distributions for piles with s_h/D of 5, at the ultimate state.

Figure 13. Development of helix bearing pressure normalized by soil undrained shear strength.

Table 1. Load test description and results.

	Test ID	t_s	s_h/D	s_g/D	Q_u (kN)	K_t (m^{-1})	Instrumentation
Pile Groups	PG-A1	7 day	3	5	401.6	N/A	N/A
	PG-B1	8 day	3	3	450.3	N/A	Piezometer
	PG-B2	5 hr	3	3	381.9	N/A	N/A
	PG-C1	9 day	3	2	507.8	N/A	Piezometer
	PG-C2	5 hr	3	2	371.0	N/A	N/A
	PG-D1[a]	8 day	5	2	N/A	N/A	Strain Gauges
	PG-D2[a]	7 day	5	2	N/A	N/A	Strain Gauges
Single Piles	P-1[b]	6 day	3	N/A	N/A	N/A	Piezometer
	P-2	15 day	3	N/A	101.5	23.4	N/A
	P-3	12 day	3	N/A	89.3	23.9	N/A
	P-4	18 day	5	N/A	93.9	22.8	Strain Gauges

Note: *a*. Load test stopped prior to reaching Q_u due to severe differential settlement; *b*. Load test without pile rotation constraint on the pile cap.

Table 2. Group pile settlements measured at the ultimate group load (Q_{ug})

Test ID	Pile Settlement (mm)			
	Pile Location			
	SW	SE	NW	NE
PG-A1	N/A[a]	10.0	15.1	20.5
PG-B1	13.2	14.2	9.6	23.9
PG-B2	13.2	8.2	18.6	21.0
PG-C1	13.6	13.8	20.7	12.9
PG-C2	22.6	16.9	14.0	7.5
PG-D1[b]	4.4	14.5	17.3	N/A[a]
PG-D2[b]	4.7	1.7	25.3	21.5

Note: *a*. pile without a functional linear potentiometer; b. Load test stopped prior to reaching Q_{ug} due to severe differential settlement.

Table 3. Comparison of measured group capacities and block failure model predicted capacities.

Test ID	s_g/D	Measured Q_{ug} (kN)	Predicted Q_{ug} (kN)	$\frac{\text{Measured } Q_{ug}}{\text{Predicted } Q_{ug}}$
PG-A1	5	402	2391	16.8%
PG-B1	3	450	1159	38.8%
PG-C1	2	508	707	71.9%

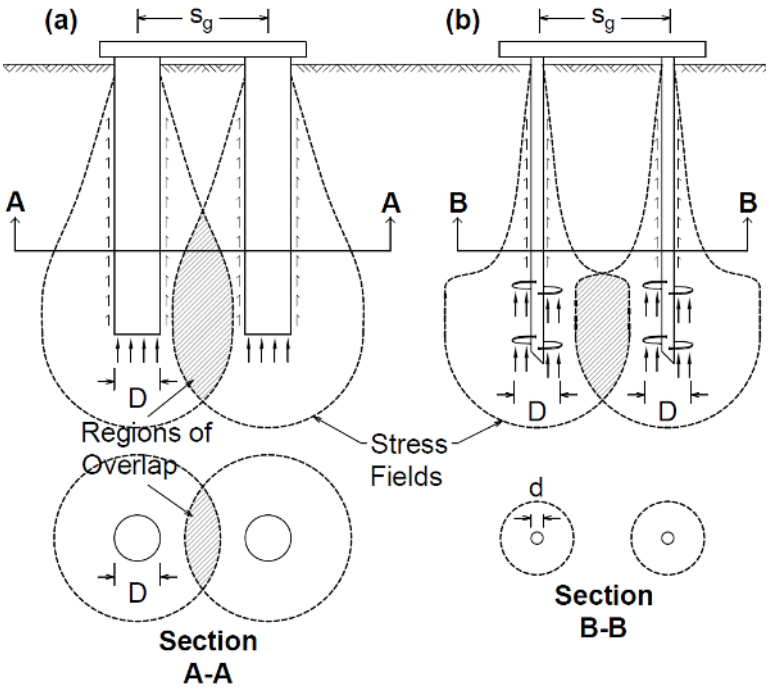

Figure 1. Conceptual schematic of stress fields around pile groups: (a) conventional pile group (adapted from Bowles 1997 and Hannigan et al. 2016); and (b) helical pile group.

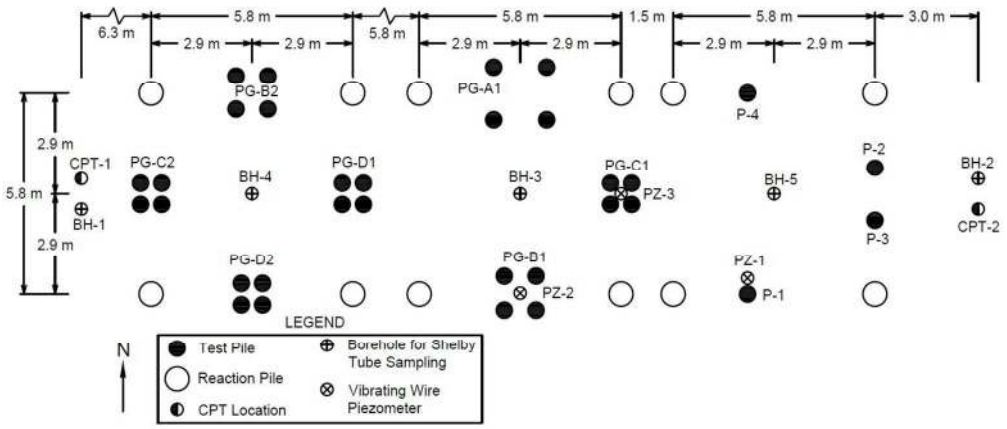

Figure 2. Test site layout and site investigation activities. Test site location: Edmonton, Canada (53°29'54" N, 113°31'57" W).

294x127mm (120 x 120 DPI)

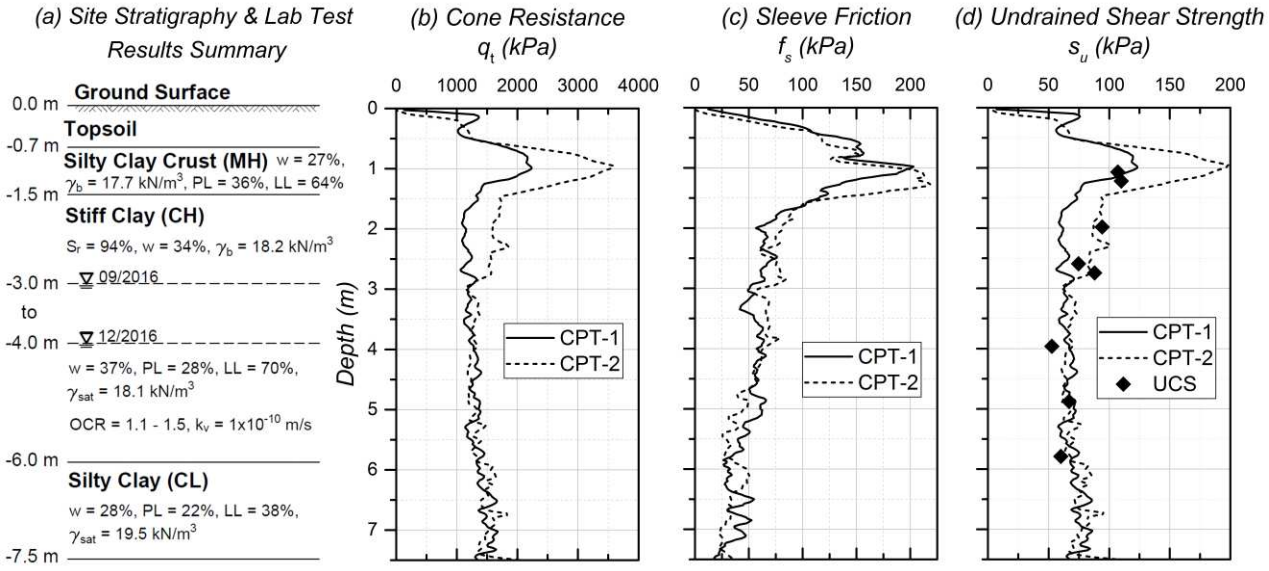

Figure 3. (a) Site stratigraphy and lab test results summary; (b) CPT cone resistance profile; (c) CPT sleeve friction profile; and (d) undrained shear strength profile.

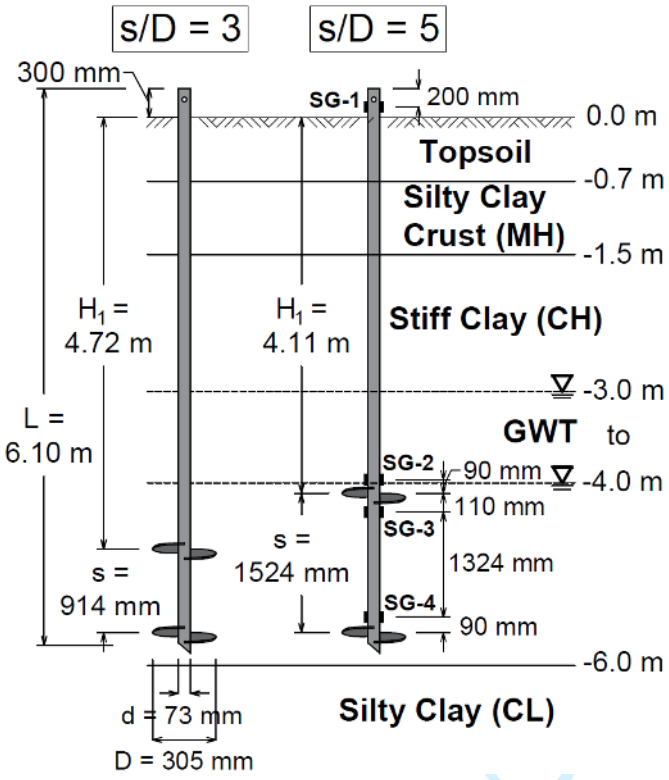

Figure 4. Test pile schematic with dimensions and strain gauge locations. Note: *L*, *d*, and *D* are equal for all test piles. Helix pitch is not drawn to scale.

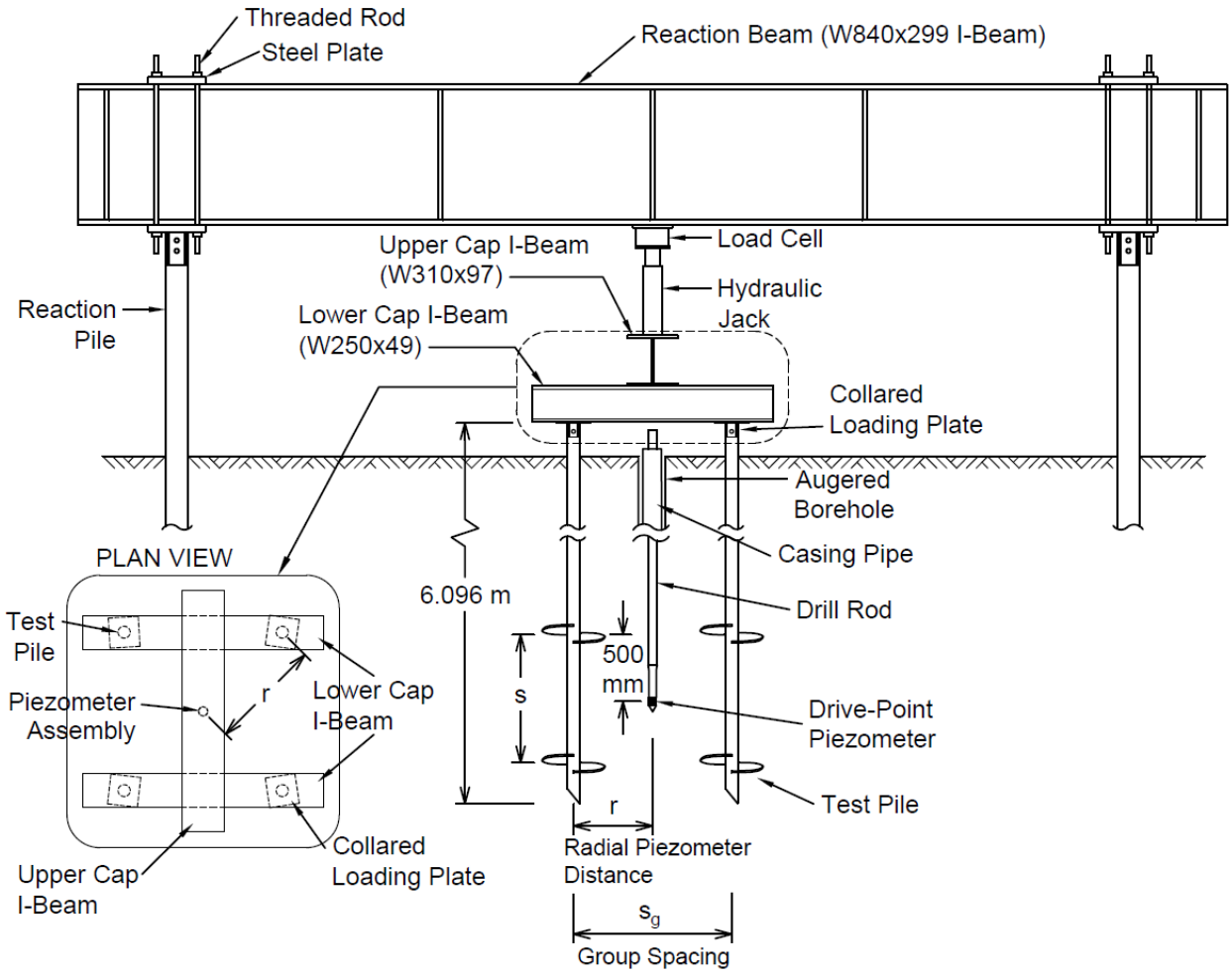

Figure 5. Pile group load test setup and piezometer assembly schematic. Note: piezometer installation for group tests PG-B1 and PG-C1 only. Same setup was used for single pile tests except that the group cap assembly was not required.

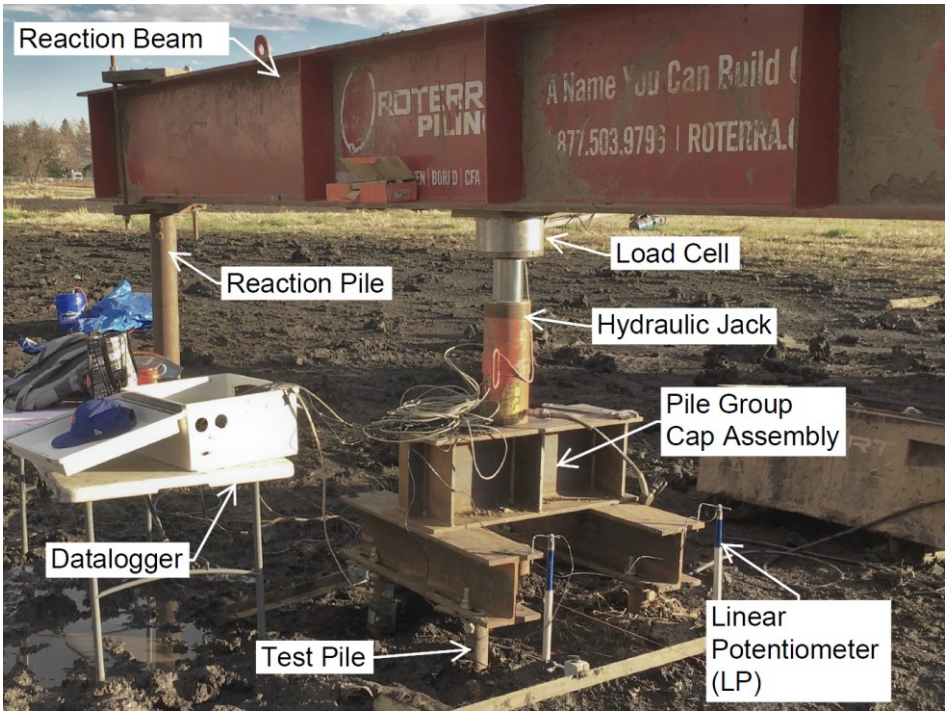

Figure 6. Photo of a typical pile group test.

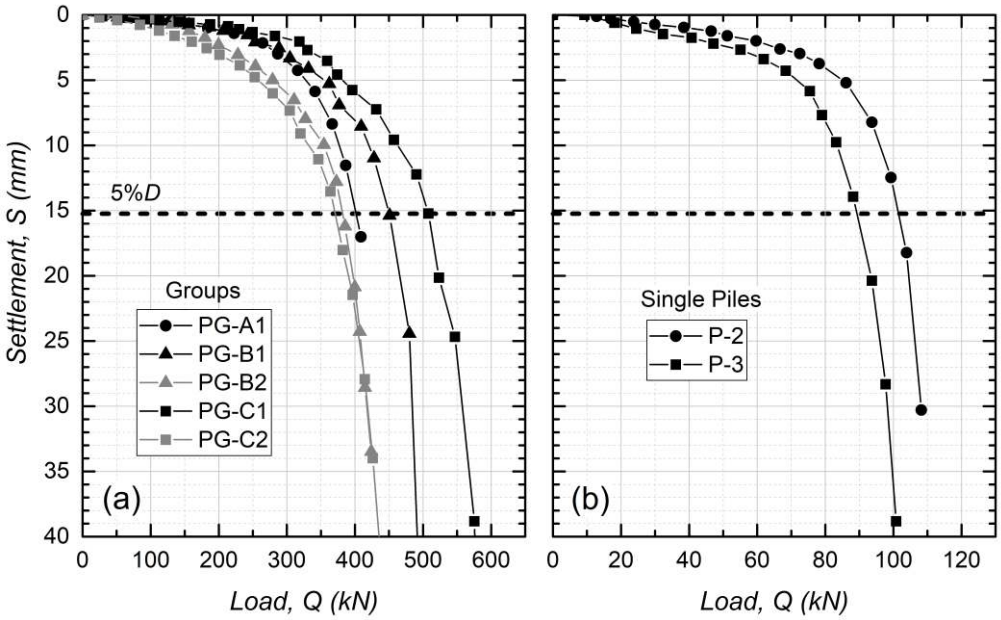

Figure 7. (a) Pile group load – settlement curves; (b) single pile load – settlement curves.

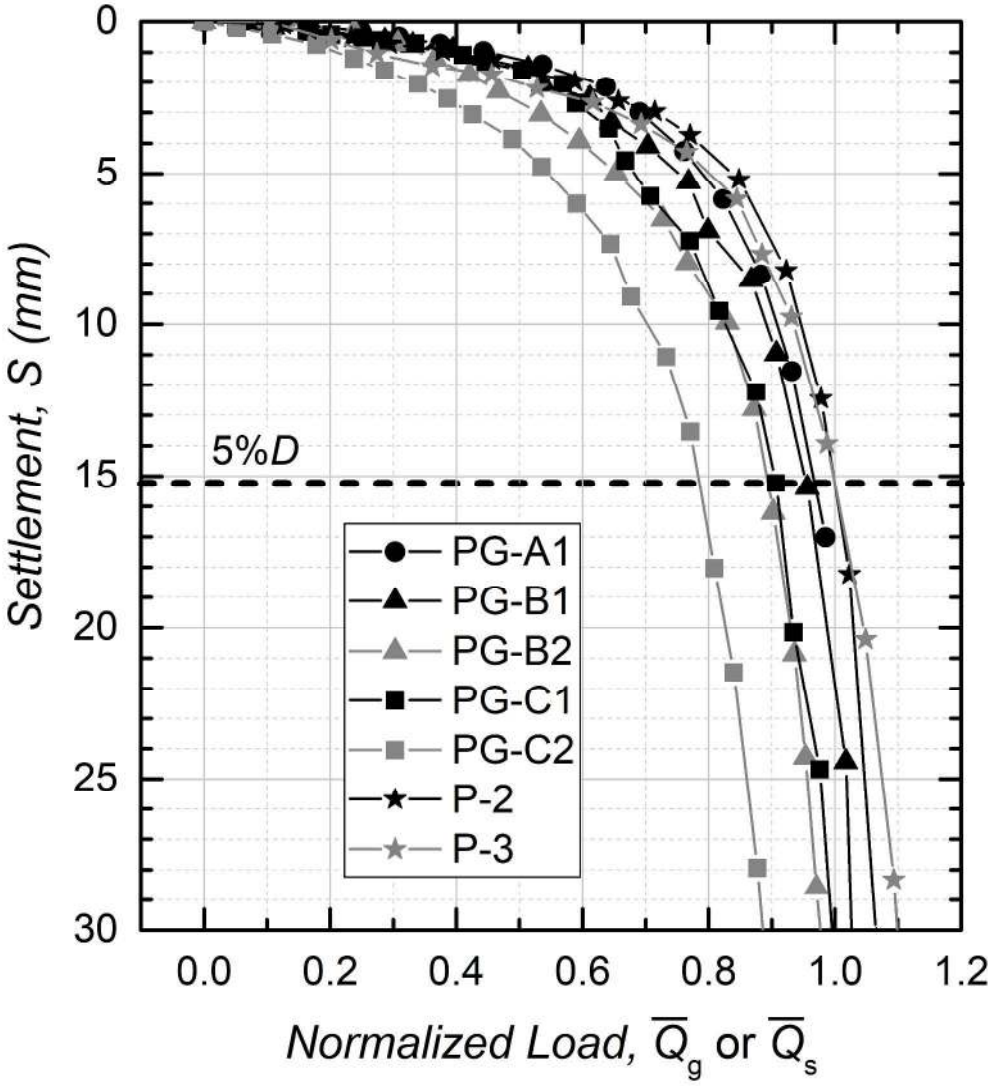

Figure 8. Pile group and single pile normalized load – settlement curves.

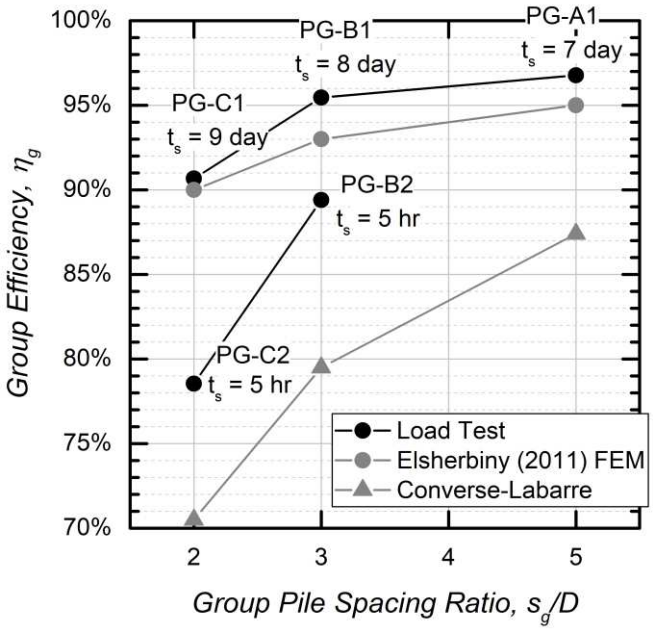

Figure 9. Group efficiency vs. group pile spacing ratio. Key parameters in Elsherbiny (2011): Q_u at $S = 5\%D$, $s_u = 75$ kPa, $L = 6.2$ m, $d = 273$ mm, $D = 610$ mm, $n = 2$, $s_h/D = 3$, and 2×2 group.

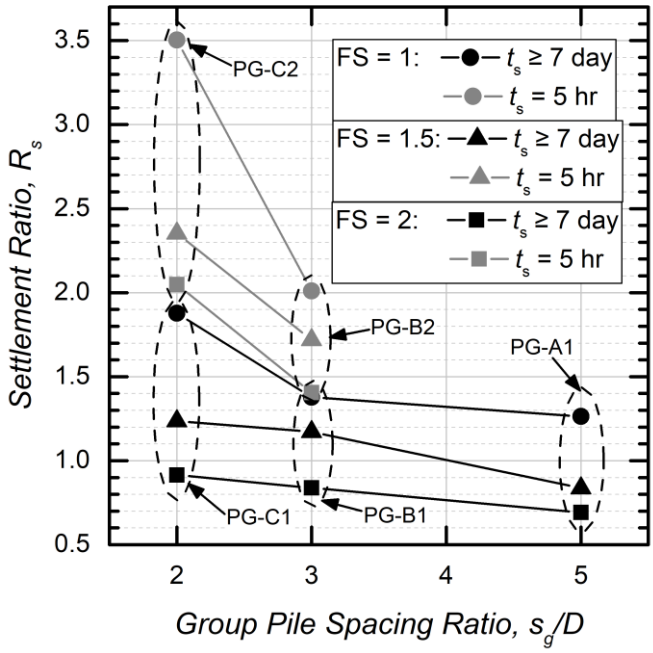

Figure 10. Settlement ratio vs. group pile spacing ratio at selected FS of pile groups.

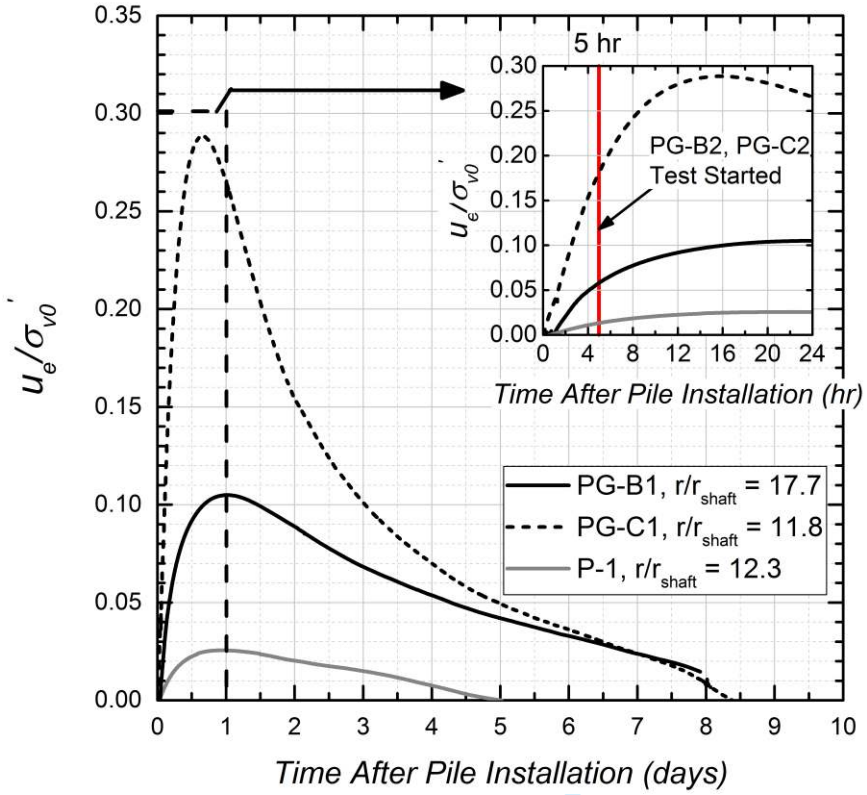

Figure 11. Installation-induced pore pressure generation and dissipation for tests PG-B1, PG-C1, and P-1. Note: Test durations of PG-B2 and PG-C2 were approximately 2 hours.

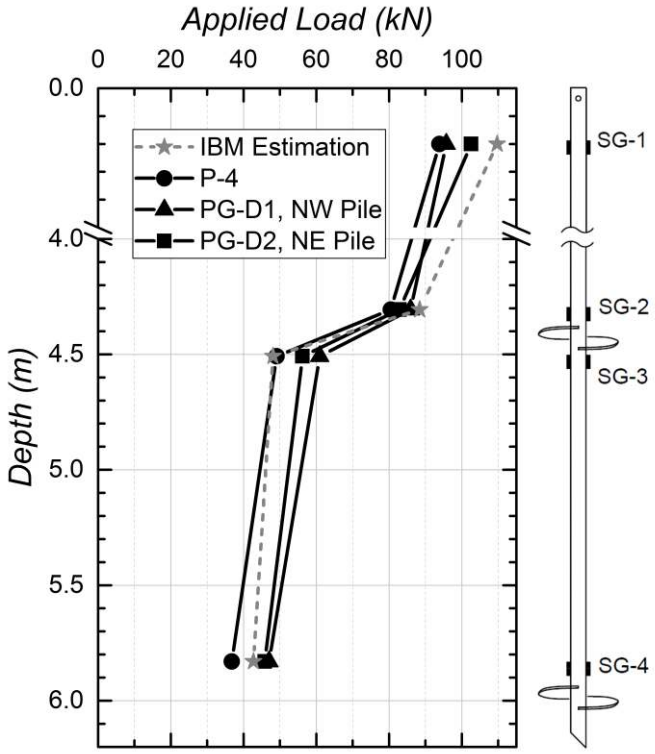

Figure 12. Measured pile load distributions for piles with s_h/D of 5, at the ultimate state.

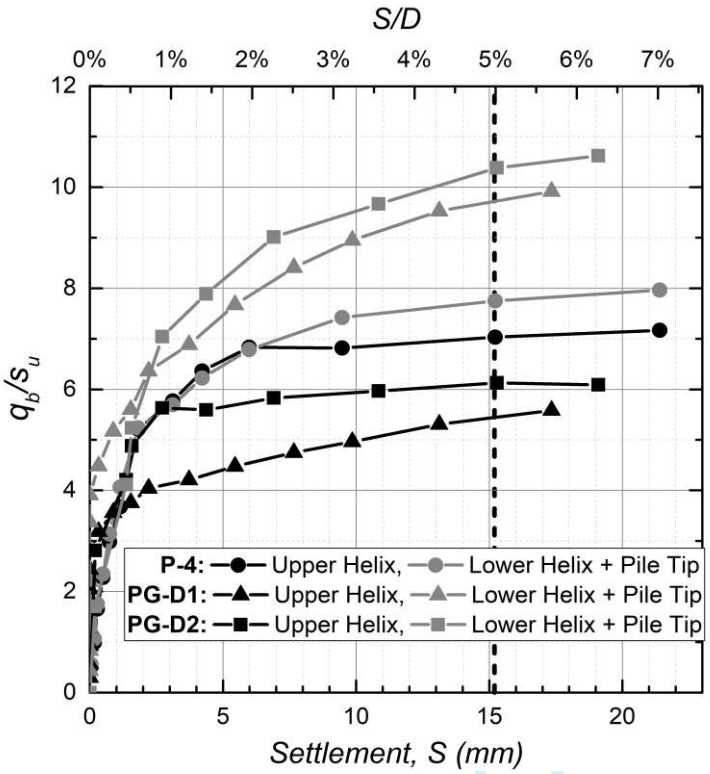

Figure 13. Development of helix bearing pressure normalized by soil undrained shear strength.